

## Simultaneous measurement of ultrasonic longitudinal wave velocities and thicknesses of a two layered media in the absence of an interface echo

Surya Prakash Kannajosyula, Vamshi Krishna Chillara, Krishnan Balasubramaniam, and C. V. Krishnamurthy

Citation: [Review of Scientific Instruments](#) **81**, 105101 (2010); doi: 10.1063/1.3494612

View online: <http://dx.doi.org/10.1063/1.3494612>

View Table of Contents: <http://scitation.aip.org/content/aip/journal/rsi/81/10?ver=pdfcov>

Published by the [AIP Publishing](#)

---

### Articles you may be interested in

[Simultaneous measurement of local longitudinal and transverse wave velocities, attenuation, density, and thickness of films by using point-focus ultrasonic spectroscopy](#)

J. Appl. Phys. **112**, 084910 (2012); 10.1063/1.4758136

[Nondestructive thickness measurement of biological layers at the nanoscale by simultaneous topography and capacitance imaging](#)

Appl. Phys. Lett. **91**, 063111 (2007); 10.1063/1.2767979

[Estimating the diameter/thickness of a pipe using the primary wave velocity of a hollow cylindrical guided wave](#)

Appl. Phys. Lett. **85**, 1077 (2004); 10.1063/1.1781353

[Simultaneous velocity and thickness imaging by ultrasonic scan](#)

AIP Conf. Proc. **557**, 695 (2001); 10.1063/1.1373825

[Time-frequency analysis of Lamb waves for distance and thickness measurement](#)

AIP Conf. Proc. **557**, 149 (2001); 10.1063/1.1373753

---

Nor-Cal Products



Manufacturers of High Vacuum  
Components Since 1962

- Chambers
- Motion Transfer
- Flanges & Fittings
- Viewports
- Foreline Traps
- Feedthroughs
- Valves



[www.n-c.com](http://www.n-c.com)  
800-824-4166

# Simultaneous measurement of ultrasonic longitudinal wave velocities and thicknesses of a two layered media in the absence of an interface echo

Surya Prakash Kannajosyula, Vamshi Krishna Chillara,  
Krishnan Balasubramaniam, and C. V. Krishnamurthy  
*Department of Mechanical Engineering, Centre for Nondestructive Evaluation, IIT Madras,  
Chennai 600 036, India*

(Received 14 September 2009; accepted 7 September 2010; published online 14 October 2010)

A measurement technique has been developed to extract the phase information of successive echoes for the simultaneous estimation of thicknesses and ultrasonic velocities of individual layers in a two layered media. The proposed method works in the absence of an interface echo and requires the total thickness of the sample to be known. Experiments have been carried out on two layered samples of white cast iron and gray cast iron with layer thickness variation in the range of 2–8 mm for total thickness variation in the range of 12–13 mm. Comparison with micrographs of a few samples confirmed the model predictions. The model is found to be sensitive to the total sample thickness but fairly insensitive to noise in the data. © 2010 American Institute of Physics.

[doi:10.1063/1.3494612]

## I. INTRODUCTION

Many methods have been used in the past for the characterization of multilayered media using ultrasound.<sup>1–6</sup> Most of these are based on the amplitude of the reflected signals from the various interfaces of the layered media. Two well known problems that have received attention in the past are (a) when the acoustic impedance mismatch between two media is such that the interface echoes are low in amplitude and are barely distinguishable from noise, and (b) when layer thicknesses are small such that weak interface echoes are overlapping with other strong interface echoes [particularly reverberations echoes from the interface at the top side (front wall) as well as between the far side, i.e., the back wall]. A third kind of problem arises when there are diffuse interface layers that do not generate any interface echo. While weak interface echoes present difficulties during signal analysis and affects the robustness of the various algorithms,<sup>4</sup> the complete absence of interface echoes (such is encountered when interfaces are diffuse) renders all such methods useless.

A new measurement method is presented here to deal with bilayered medium with a diffuse interface layer that does not produce any interface echo. The method utilizes the phase delay between the front-wall echo and the back-wall echo caused by pulse propagation at normal incidence. This phase delay is made up of wave propagation in the two media and across the extent of the diffuse interface. Keeping in mind that the spatial extent of the diffuse interface would be in micron and submicron length scales, and considering that layer thicknesses need to be ascertained to within 1 mm or so, it is proposed that the diffuse interface be regarded as a pseudointerface, a partition, that separates the two layers in an average sense. A simple search in a three-parameter space, namely, the thickness of one layer and the propagation ve-

locities in the two layers is carried out to optimize the phase delay in the least squares sense. The method is applied to a bilayer medium consisting of gray cast and white cast iron. Simulations are validated with experiments and the method is shown to work for white cast iron thicknesses ranging from 2 to 8 mm. The method is shown to be reasonably robust against typical noise levels encountered in the experiment and effects of typical experimental errors in the time of arrival of the back-wall signal. While the present method employs a simple search in the parameter space, it is hoped that more sophisticated search options would be more helpful in dealing with more complex multilayered media.

The paper is organized as follows. The method is presented in Sec. II. Experiments carried out on several samples are described in Sec. III. Results and discussion are given in Sec. IV followed by conclusions.

## II. APPROACH

The objective is to estimate the thicknesses of the white cast iron and gray cast iron portions of the specimen, given the specimen's total thickness. This is accomplished by approximating the problem using a bilayer model. A bilayered media is considered to be made up of two materials A and B such that the interface does not produce any measurable signal in a commonly used immersion mode ultrasonic pulse-echo configuration. Figure 1 shows a schematic of the configuration under consideration.

A broadband signal is considered to propagate through the bilayered medium, producing a front-wall echo due to the acoustic impedance mismatch between water—medium A and back-wall echo between medium B—water, respectively. Dispersion effects are unlikely in these materials and hence not considered.

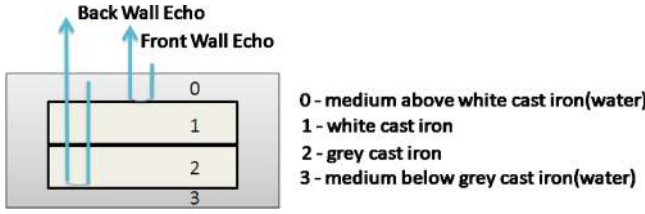


FIG. 1. (Color online) Schematic showing multiple reflections within the sample.

The effective reflection coefficient is evaluated for the bilayered medium for each of the frequencies present in the broadband signal assuming plane wave propagation. Following Refs. 7 and 8, the effective reflection coefficient in frequency domain for the configuration shown in Fig. 1 is obtained in two steps. In the first step, the effective reflection coefficient is obtained by considering second and third layers as

$$R_{12\text{net}} = R_{12} + \frac{T_{12}R_{23}T_{21}e^{-2i(k_2d_2)}}{1 - R_{23}R_{21}e^{-2i(k_2d_2)}}, \quad (1)$$

where  $R_{12\text{net}}$  is the effective reflection coefficient at the interface between 1 and 2 involving media 2 and 3. In the second step, the effective reflection coefficient for the entire block shown in Fig. 1 is obtained as (see the Appendix for the derivation)

$$R_{\text{net}} = R_{01} + \frac{T_{01}R_{12\text{net}}T_{10}e^{-2i(k_1d_1)}}{1 - R_{12\text{net}}R_{10}e^{-2i(k_1d_1)}}, \quad (2)$$

where  $R_{ij}$  and  $T_{ij}$  are the reflection and transmission coefficients between media  $i$  and  $j$ , respectively,  $d_1$  and  $d_2$  are the individual layer thicknesses,  $k_1$  and  $k_2$  are the wave numbers corresponding to the  $P$ -waves in the individual layers. The factor 2 accounts for the two-way propagation of the wave.

The expression accounts for all the multiple echoes, when inverted to the time domain and is limited only by the experiment. As only the first two back-wall echoes are of current interest, the expression for the effective reflection coefficient for the configuration in Fig. 1 is expanded as a truncated series.

$$R_{\text{net}} = R_{01} + T_{01}T_{10}(T_{12}R_{23}T_{21})e^{-2i(k_1d_1+k_2d_2)} + T_{01}T_{10}(T_{12}R_{23}T_{21})^2R_{10}e^{-4i(k_1d_1+k_2d_2)}. \quad (3)$$

The effective reflection coefficient above deals with the front-wall echo followed by the first two back-wall echoes without an interface echo.

The phase delay between the front-wall echo and the first back-wall echo shows up as the factor  $e^{-2i(k_1d_1+k_2d_2)}$  in the last term of the truncated series. In this phase factor, there are three unknowns:  $d_1$ , the thickness of one of the layers and  $v_1$  and  $v_2$  the two longitudinal velocities in the two layers. The proposed method seeks to estimate these three unknowns through a least-square search algorithm in the parameter space, assuming that the ranges of values for each of these unknowns are known *a priori*. Specifically,

- Let  $Y_1$  and  $Y_2$  be the vectors denoting time domain pulses of first and second back-wall echoes. Let  $y_1$  and  $y_2$  be their

corresponding discrete Fourier transform vectors, which contain complex entries and are of same length as that of the time domain pulses.

- Let  $f$  be the vector corresponding to the frequencies present in the time domain signals.
- Let  $d$  denote the total thickness of two layers.  $d_1$  and  $d_2$  denote the thicknesses of the first and second layer. ( $d_1 + d_2 = d$ )  $d_1 \in R^+$ ,  $d_2 \in R^+$  which we seek to determine.
- Let  $v_1$  and  $v_2$  denote the velocity of ultrasonic waves in these two media and  $k_1$  and  $k_2$  denote the wave numbers in the media.  $v_1 \in R^+$ ,  $v_2 \in R^+$  which we seek to determine.

The Fourier transforms  $y_1$  and  $y_2$  are individually normalized to get a set of new vectors  $y_{11}$  and  $y_{22}$ . That is

$$y_{11}(j) = \frac{y_1(j)}{|y_1(j)|} \quad \text{for } j = 1, 2, \dots, N, \quad (4)$$

where  $N = \text{length of the vectors } y_1, y_2$

$$y_{22}(j) = \frac{y_2(j)}{|y_2(j)|} \quad \text{for } j = 1, 2, \dots, N. \quad (5)$$

Another vector  $e^{i\phi}$  is obtained by element wise division of  $y_{22}$  by  $y_{11}$ .

$$e^{i\phi}(j) = \frac{y_{22}(j)}{y_{11}(j)} \quad \text{for } j = 1, 2, \dots, N. \quad (6)$$

This vector  $e^{i\phi}$  should be equal to  $e^{-2i(k_1d_1+k_2d_2)}$  at each of the frequencies in the broadband signal apart from a  $180^\circ$  phase change that is unrelated to the phase change caused by wave propagation across the bilayer medium. The  $180^\circ$  phase change at the back wall due to the wave undergoing reflection from a medium of lower impedance is removed from both the simulated signals and the experimental signals in the Fourier domain. As experimental signals have noise in amplitude and phase, the measured phase change  $\phi$  may not agree exactly with the phase factor  $(k_1d_1+k_2d_2)$ . Also the measured phase change  $\phi$  has a possibility of differing from actual phase change ( $\phi_{\text{expt}}$ ) by  $2n\pi$  where  $n$  is an integer. Explicitly, if  $\phi$  is the measured phase, it differs from the actual phase change in the experiment ( $\phi_{\text{expt}} = k_1d_1+k_2d_2$ ) by  $2n\pi$ , i.e.,  $\phi = \phi_{\text{expt}} + 2n\pi$  where  $n$  is an integer. Using  $e^{i\phi}$  eliminates such ambiguity as  $e^{i\phi} = e^{i(\phi+2n\pi)}$ . Also it is expected that the use of  $e^{i\phi}$  indirectly refers to use of both  $\cos(\phi)$  and  $\sin(\phi)$  as objective functions simultaneously and hence imposing a stronger condition on optimization.

A least square error objective function ( $G$ ) is defined in three parameters, namely,  $d_1$  (or  $d_2$ ),  $v_1$ , and  $v_2$  as

$$G(d_1, v_1, v_2) = F(d_1, v_1, v_2) \times F(d_1, v_1, v_2)^\dagger \quad (7)$$

where

$$F(d_1, v_1, v_2) = e^{-2i(k_1d_1+k_2d_2)} - e^{i\phi}$$

and  $F^\dagger$  is the complex conjugate transpose of  $F$ .

The objective function ( $G$ ) is sought to be minimized by using any of the various search methods or gradient based algorithms to obtain the three unknown parameters. It may be noted that the range of frequencies over which the algorithm operates is practically determined by the spectral win-

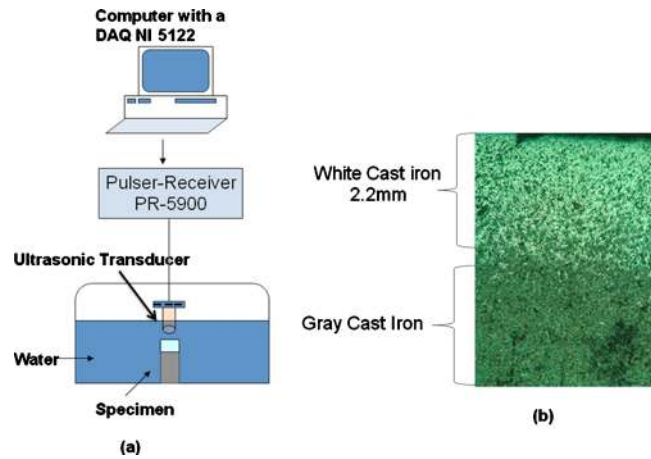


FIG. 2. (Color online) Schematic diagram of the (a) experimental setup. (b) Micrograph of one of the samples (2 mm) showing the white cast and gray cast portions (diffuse interface may be noted).

dow for which the Fourier coefficients are nonzero for the received signal, rather than the entire bandwidth of the original input signal.

The algorithm is tested on data generated using simulation using a four-layer stack consisting of water-white cast iron-gray cast iron-water with an input pulse taken to be a Gaussian pulse of the form

$$S = Ae^{-\alpha(t-\tau)^2} \sin[2\pi f_c(t-\tau) + \phi], \quad (8)$$

where  $A$  has been set to unity,  $\phi$  is set to zero, and the center frequency is taken to be 5 MHz. The bandwidth factor is set to 80% and the pulse is centered at 1  $\mu$ s.

The front-wall echo and the back-wall echo are generated for various combinations of  $d_1, v_1, v_2$  over a range of values for each of the unknowns. It is known that the longitudinal wave velocity in cast iron depends upon the size and quality of the internally distributed graphite, thus leading to its variability across samples.<sup>9</sup> Accordingly, a range of longitudinal wave velocities for gray cast and white cast iron media was arrived at using experimental values obtained for a set of test samples of white cast iron and gray cast iron and the range of values reported in the literature.<sup>9</sup> Specifically, these ranges were taken to be from 4.9 to 5.00 mm/ $\mu$ s for gray cast iron, and from 5.90 to 6.05 mm/ $\mu$ s for white cast iron, respectively. White cast iron layer thickness range was considered to lie between 2 and 8 mm for the set of samples provided by the manufacturer. A least square error objective function is evaluated involving all the frequencies within the chosen bandwidth for each of the above combinations and the combination which returns the least value of this function is considered to be the solution. A simple linear search was carried out to determine the solution. Simulations were carried out using MATLAB on a personal computer (PC) with 256 MB random access memory.

### III. EXPERIMENTS AND DATA ANALYSIS

The schematic for the experimental set up is shown in Fig. 2. It consists of a 0.375 in. diameter planar immersion transducer with 5 MHz center frequency placed at about 50 mm from the sample's front surface. A Panametrics

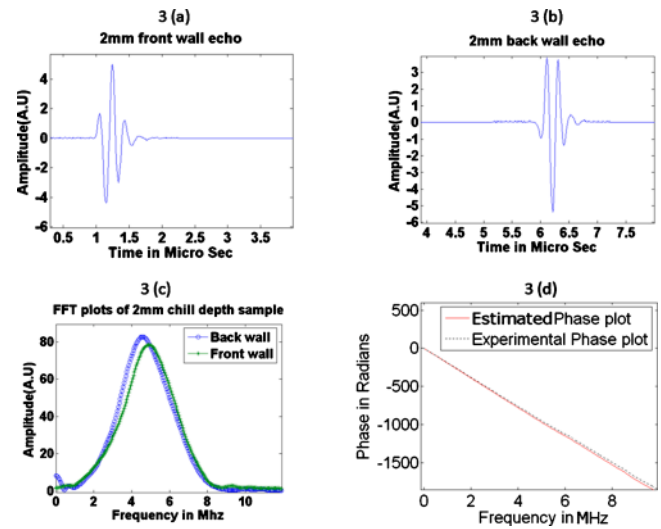


FIG. 3. (Color online) (a) Front-wall echo and (b) first back-wall echo, (c) FFTs of front-wall echo and back-wall echoes, and (d) estimated and experimental phase plots.

Pulser-Receiver 5800 is used to transmit and receive pulses. A National Instruments data acquisition card, NI 5122, is used to collect the data at a sampling frequency of 100 MHz and a PC is used to store and process the signal records.

The samples provided by the manufacturer had the average thickness of the white cast iron layer ranging from 2 to 8 mm. Figure 2(b) shows the micrograph of one of the samples indicating that the top layer thickness is not strictly constant across the lateral dimension of the sample.

Signals are shown for two samples, one having higher gray cast iron, less white cast iron and other one having lower gray cast iron and higher white cast iron. Each signal record consists of the front-wall echo and the first back-wall echo with adequate zero padding ahead of the front-wall echo and behind the first back-wall echo. For purposes of evaluating the fast Fourier transform (FFT) of one of these echoes, the rest of the signal was replaced by zeroes in the

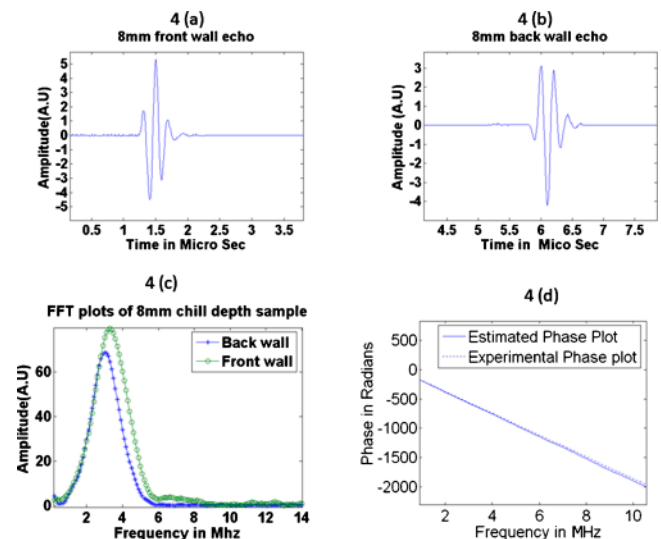


FIG. 4. (Color online) (a) The rf signal representing the front-wall echo and (b) first back-wall echo, (c) FFTs of front-wall echo and back-wall echoes, and (d) estimated and experimental phase plots.

TABLE I. Showing the chill depth estimates for the samples of various chill depths.

Chill depth of samples (mm)	Total thickness ( $d$ ) (mm)	Estimated thickness of white cast iron ( $d_1$ ) (mm)	Estimated velocity in white cast iron ( $v_1$ ) (mm/ $\mu$ s)	Estimated velocity in gray cast iron ( $v_2$ ) (mm/ $\mu$ s)	Percent error in estimated thickness of white cast iron
2	12.3	2.0	5.96	4.97	0.00
3	12.7	2.0	5.91	4.98	-33.33
4	12.6	3.5	5.95	4.99	-12.50
5	12.6	5.5	5.97	4.93	10.00
6	12.6	7.0	5.96	4.92	16.67
8	12.5	8.5	5.95	4.94	6.25

time domain keeping the total signal record length the same as the original record having both the echoes. Figures 3(a) and 3(b) show gated portions of the two echoes separately. While calculating  $y_{11}$  and  $y_{22}$ , frequency components of only a fixed bandwidth are considered. This bandwidth depends on the transducer bandwidth. The FFT of the front wall signal was gated for the required bandwidth and for the same frequencies, frequency components of the first back-wall echo were extracted and used in the algorithm for calculation. The signals shown in Fig. 3 are for a 2 mm chill depth sample with  $d=12.3$  mm. The signals shown in Fig. 4 are for an 8 mm chill depth sample with  $d=12.5$  mm.

Two different gain settings, 20 and 40 dB, were used to extract the front-wall signal and back-wall signals, respectively, to obtain a back-wall signal with good signal-to-noise ratio (SNR) and to avoid the saturation of the front-wall signal.

While calculating  $y_{11}$  and  $y_{22}$ , frequency components of only a fixed bandwidth were considered. This bandwidth depends on the transducer bandwidth and material attenuation. It has been observed that the attenuation in the back-wall signals, due to the presence of gray cast iron, resulted in a shift in the peak of the FFT spectrum toward lower frequencies [see Figs. 3(c) and 4(c)] as one moves toward lower chill depths. The FFT spectrum of the unattenuated front-wall signal was gated for the required bandwidth and for the same frequencies, frequency components of the first back-wall echo are extracted and used in the algorithm for calculation.

Experimental data with varying signal record lengths were used and it has been observed that the parameters estimated with FFT are independent of the overall record length. Sampling rate of at least 100 MHz was found to be necessary for evaluating the spectral features. It may be noted that zero padding ahead of the front wall or behind the first back wall has the effect of a constant phase shift on each of the echoes and does not influence the final outcome.

#### IV. RESULTS AND DISCUSSIONS

The results of the chill depth estimates for the six samples are presented in tables. In Table I, the chill depth values in the first column are provided by the manufacturer and are based on random destructive tests combined with acid treatment (etching) on the sides of the bilayered sample. As is known, the chill depth is not expected to be a constant across the cross-section. However, given that plane wave calculations are carried out based on the far-field beam characteristics of the transducer, what is extracted through the proposed method may be regarded as the layer thickness averaged over the specimen cross-section. Further, as it is known that the interface layer is diffuse and not sharply defined, the layer thickness can only be approximately defined to within 1 mm. From Table I, it can be seen that the method works reasonably well. It is worth noting that the distribution of the estimates for the wave velocities in the individual layers is fairly narrow.

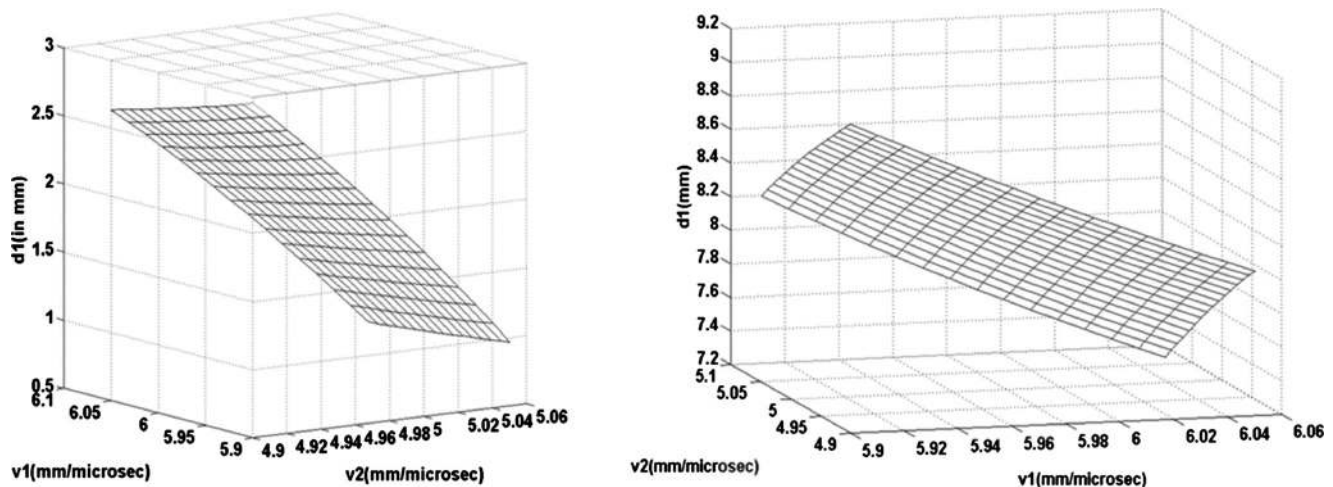
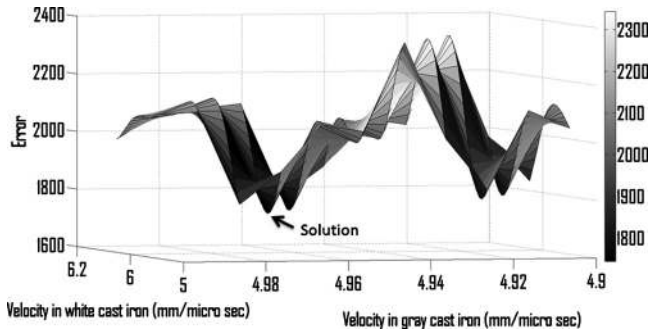


FIG. 5. Solution surfaces at (a) 2 mm and (b) 8 mm chill depths.

FIG. 6. Plot of objective function ( $G$ ) for  $d_1=2$  mm.

Three constraints act to restrain the search to produce correct solutions—measured phases, total thickness, and range of possible values of  $v_1, v_2$ . Also, time lapse due to pulse propagation within the bilayered medium is required to be satisfied at each frequency within the chosen bandwidth in terms of the corresponding phase change and can be written as

$$\frac{d_1}{v_1} + \frac{d_2}{v_2} = \left[ \frac{\Phi(\omega)}{2\omega} \right]_{\text{frequencies in bandwidth}}. \quad (9)$$

Given that the total thickness is obtained from an independent measurement, and given that the experimental phase change, namely, the values of  $[\Phi(\omega)/2\omega]$  lie scattered in a finite range about some mean, the solution domain in the three-dimensional-space corresponding to the three unknowns ( $d_1, v_1, v_2$ ) is found to take the form of an inclined and slightly twisted surface for each frequency. Figures 5(a) and 5(b) depict such surfaces for 2 and 8 mm chill depth cases at one of the frequencies within the chosen bandwidth. The first characteristic of these solution surfaces is that these surfaces are found to lie within a narrow domain of values for  $d_1$ . This domain can be visualized as a slab whose thickness is governed by the domain of values for  $d_1$  and whose other dimensions are governed by the domains over which the velocity range is considered. For a given chill depth, for each frequency, a slab exists within which a solution surface is confined. When viewed over the entire bandwidth, slabs for different frequencies would be overlapping giving rise to a common volume. Solution surfaces within these slabs lie in proximity of each other in the least square sense. The second characteristic is that as the chill depth increases, the slab is found to be narrower in the thickness dimension due to solutions lying in a narrower range of values for  $d_1$ . For instance, for the 2 mm chill depth case, the  $d_1$  values are confined between 1 and 3 mm and for the 8 mm chill depth case,

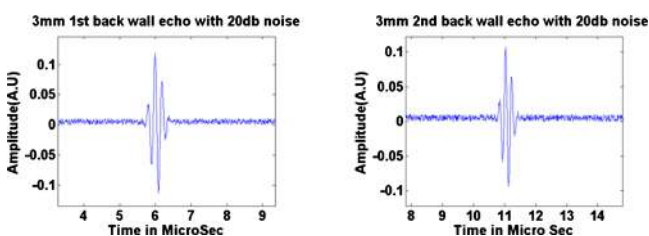


FIG. 7. (Color online) (a) First back wall and (b) second back-wall echo of a 3 mm chill depth sample with 20 dB noise level.

TABLE II. Estimated parameters with 20 dB noise.

Actual thickness of white cast iron (mm)	Estimated thickness of white cast iron (mm)	Estimated velocity in white cast iron (mm/ $\mu$ s)	Estimated velocity in gray cast iron (mm/ $\mu$ s)
2.00	1.60	5.98	4.96
3.00	3.50	5.97	4.93
4.00	3.60	5.98	5.00
5.00	4.80	6.01	4.98
6.00	5.80	6.04	4.98
8.00	7.60	6.04	4.99

the  $d_1$  values are confined only between 7.4 and 8.6 mm. These two characteristics of the solution domain ensure that the range of possible solutions is limited for each chill depth case and enables an appropriate  $d_1$  to be determined within 1 mm in the least square sense along with the corresponding values for the wave speeds in the two media. The search procedure adopted amounts to discretization using surfaces in the common volume of intersecting slabs by planes  $d_1 = \text{const}$  separated by 0.5 mm (step size of the search along  $d_1$ ), evaluating the objective function  $G$  and determining a triad ( $d_1, v_1, v_2$ ) as a solution. For instance the plot of objective function ( $G$ ) at one such plane  $d_1=2$  mm is shown in Fig. 6.

A simple search was adopted to identify the solution by determining the lowest value of the objective function ( $G$ ) in the constrained solution space. While it is possible to use other search methods to arrive at the solution such as genetic algorithm based optimization procedures,<sup>10</sup> the existence of multiple minima precludes use of gradient based search methods (Fig. 6).

### A. Effect of noise level on the estimated parameters

The effect of white noise on the estimated parameters was investigated. Signals were simulated with an added noise (amplitude scale) of 20 and 40 dB (Fig. 7) for the case  $d=13$  mm,  $d_1=2$  mm,  $v_1=6$  mm/ $\mu$ s, and  $v_2=4.95$  mm/ $\mu$ s. These noise levels were typically more than what was observed in experiments. It was observed that the model is very robust to the amount of noise typically encountered in these samples (Tables II and III).

TABLE III. Estimated parameters with 40 dB noise.

Actual thickness of white cast iron (mm)	Estimated thickness of white cast iron (mm)	Estimated velocity in white cast iron (mm/ $\mu$ s)	Estimated velocity in gray cast iron (mm/ $\mu$ s)
2.00	1.80	5.97	4.96
3.00	3.20	5.96	4.92
4.00	3.50	6.03	4.99
5.00	4.80	6.01	4.98
6.00	6.10	6.05	4.92
8.00	7.40	6.04	4.98

TABLE IV. Showing the effect of thickness measurement on the estimated parameters for a total thickness  $d=13$  mm,  $v_1=6$  mm/ $\mu$ s,  $v_2=4.95$  mm/ $\mu$ s, and  $d_1=4$  mm.

S. No.	Total thickness ( $d$ ) (mm)	Estimated thickness of white cast iron ( $d_1$ ) (mm)	Estimated velocity in white cast iron ( $v_1$ ) (mm/ $\mu$ s)	Estimated velocity in gray cast iron ( $v_2$ ) (mm/ $\mu$ s)	Error in estimated thickness of white cast iron (mm)
1	12.60	2.50	5.90	4.90	-1.50
2	12.70	2.50	6.01	4.93	-1.50
3	12.80	3.00	5.94	4.95	-1.00
4	12.90	3.00	5.99	4.99	-1.00
5	13.00	4.00	6.00	4.95	0.00
6	13.10	4.50	5.91	4.99	0.50
7	13.20	5.50	6.00	4.91	1.50
8	13.30	6.00	5.94	4.95	2.00
9	13.40	6.50	5.99	4.93	2.50

## B. Sensitivity of chill depth estimates to errors in total thickness data

The total thickness  $d$  was found to be a very important factor for this model. The estimation of chill depth was found to be quite sensitive to the total thickness. An error of 4%–5% in total thickness measurement will result in an error of 55%–60% error in thickness and velocities estimation. Results of simulation are presented here (Table IV) for total thickness  $d=13$  mm and thickness of white cast ( $d_1$ ) =4 mm,  $v_1=6$  mm/ $\mu$ s, and  $v_2=4.95$  mm/ $\mu$ s. Table IV below shows the change in estimation of parameters with respect to the change in error of thickness measurement. The error in total thickness measurement to the error in estimated thickness of the white cast iron is shown in Fig. 8.

Figure 8 shows graphically the error in the estimation of the thickness of the white cast iron due to the error in the total thickness measurement. The origin of the slight asymmetry seen in the error trends in the two quadrants is unclear.

## V. CONCLUSIONS

A new measurement technique was developed for estimating the layer thicknesses and ultrasonic longitudinal wave velocities in a two layered media with a diffuse interface by exploiting the phase information in the complete absence of an interface echo. The technique is based on one-dimensional wave propagation describing a plane wave at

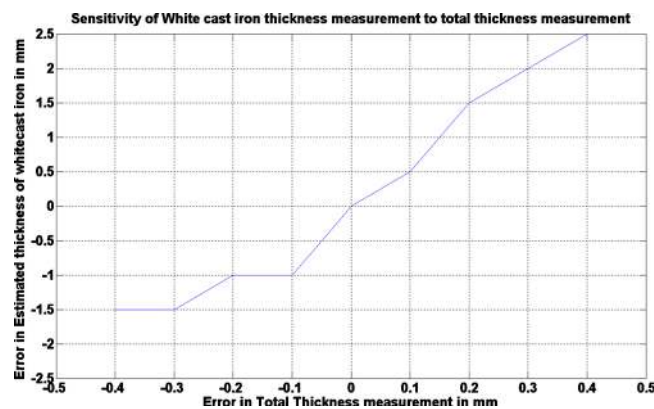
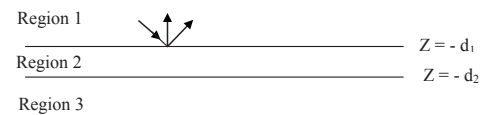


FIG. 8. (Color online) Sensitivity of layer thickness estimation to errors in total thickness measurement.

normal incidence through a two layered sample. It assumes that the total thickness of the sample is known. Experiments were carried out using an ultrasonic immersion technique over a range of layer thicknesses. The measurement method was found to be robust to the noise present in the signal but is very sensitive to the total thickness of the sample.

The “correctness” is inferred from the numerous trials carried out using simulations and conducting experiments on a range of specimens. The method is general in that it works even in the presence of an interface echo with the advantage that even a weak interface echo increases its efficiency and improves its robustness. However, it is not expected to yield solutions when the diffuse interface is within 1 mm of the front wall or the back wall. Such diffuse interfaces close to the front wall (or to the back wall) pose additional challenges due to contamination of front or back-wall echoes. Attempts to deal with these challenges are under way.

## APPENDIX: EFFECTIVE REFLECTION COEFFICIENT OF A THREE LAYERED MEDIUM



Consider a three layered media as shown above. Assume a planar wave is normally incident on the interface between region 1 and region 2. The wave in region 1 can therefore be written as

$$e_{1y} = A_1 [e^{-ik_1z} + \tilde{R}_{12} e^{(2ik_1z d_1 + ik_1z)}], \quad (A1)$$

where  $\tilde{R}_{12}$  is a reflection coefficient that is the ratio of the up going wave amplitude and the down going wave amplitude at the first interface  $z=-d_1$ .

The wave in region 2 has similar form

$$e_{2y} = A_2 [e^{-ik_2z} + R_{23} e^{(2ik_2z d_2 + ik_2z)}], \quad (A2)$$

where  $R_{23}$  is the Fresnel reflection coefficient for a down going wave in region 2 reflected by region 3 because region 3 extends to infinity in the  $-z$  direction. The wave in region 3 can be written as

$$e_{3y} = A_3 e^{-ik_3 z}. \quad (\text{A3})$$

The unknowns  $A_1$ ,  $A_2$ ,  $A_3$ , and  $\tilde{R}_{12}$  are found by imposing constraint conditions at the interfaces. First, by tracing the propagation of waves, it is noted that the down going wave in region 2 is a consequence of the transmission of the down going wave in region 1 plus a reflection of the up going wave in the region 2; that is, at the top interfaces,  $Z = -d_1$ , the constraint conditions is

$$A_2 e^{ik_2 z d_1} = A_1 e^{ik_1 z d_1} T_{12} + R_{21} A_2 R_{23} e^{(2ik_2 z d_2 - ik_2 z d_1)}. \quad (\text{A4})$$

The first term in Eq. (A4) is the transmission of the down going wave amplitude in region 1 at  $z = -d_1$ , i.e.,  $A_1 e^{ik_1 z d_1}$  via the Fresnel transmission coefficient  $T_{12}$ . The second term is the reflection of the up going wave amplitude in the region 2 at  $z = -d_1$ , i.e.,  $A_2 R_{23} e^{(2ik_2 z d_2 - ik_2 z d_1)}$ . via the Fresnel coefficient  $R_{21}$ .

Next, it is noted that the upward traveling wave in region 1 is caused by the reflection of the downward traveling wave in region 1 plus a transmission of the upward traveling wave in region 2. Consequently, at the interface  $z = -d_1$ , we have the constraint condition

$$A_1 \tilde{R}_{12} e^{ik_1 z d_1} = A_1 R_{12} e^{ik_1 z d_1} + T_{21} A_2 R_{23} e^{(2ik_2 z d_2 - ik_2 z d_1)}. \quad (\text{A5})$$

From the above equation  $A_2$  can be solved for in terms of  $A_1$ , yielding

$$A_2 = \frac{T_{12} A_1 e^{i(k_1 z - k_2 z) d_1}}{1 - R_{21} R_{23} e^{2ik_2 z (d_2 - d_1)}}. \quad (\text{A6})$$

Then, substituting Eq. (A6) into Eq. (A5) we obtain

$$\tilde{R}_{12} = R_{12} + \frac{T_{12} R_{23} T_{21} e^{2ik_2 z (d_2 - d_1)}}{1 - R_{21} R_{23} e^{2ik_2 z (d_2 - d_1)}}. \quad (\text{A7})$$

Here  $\tilde{R}_{12}$  is the generalized reflection coefficient for the three layered medium that relate the amplitude of the up going wave to the amplitude of the down going wave in region 1. It

includes the effect of subsurface reflection as well as the reflection from the interface.

To elucidate the physics better, the above equation can be expanded in terms of a series

$$\begin{aligned} \tilde{R}_{12} = & R_{12} + T_{12} R_{23} T_{21} e^{2ik_2 z (d_2 - d_1)} + T_{12} R_{23}^2 T_{21} e^{4ik_2 z (d_2 - d_1)} \\ & + \dots \end{aligned} \quad (\text{A8})$$

Now if an additional layer is added below region 3, we need only replace  $R_{23}$  in Eq. (A7) by  $\tilde{R}_{23}$ , for previous derivation,  $R_{23}$  is the ratio between up going and down going wave amplitudes in region 2. Therefore, if a subsurface layer is added in region 3, this ratio will just become  $\tilde{R}_{23}$ .

$$\tilde{R}_{\text{net}} = R_{12} + \frac{T_{12} \tilde{R}_{23} T_{21} e^{(-2ik_1 d_1)}}{1 - \tilde{R}_{23} R_{21} e^{-2ik_1 d_1}} \quad (\text{A9})$$

With the numbering system followed in Fig. 1 of the paper Eq. (A9) can be written as

$$R_{\text{net}} = R_{01} + \frac{T_{01} R_{12\text{net}} T_{10} e^{[-2i(k_1 d_1)]}}{1 - R_{12\text{net}} R_{10} e^{[-2i(k_1 d_1)]}}. \quad (\text{A10})$$

<sup>1</sup>J. P. Zhang and Y. Wei, *Acoust. Imaging* **15**, 571 (1987).

<sup>2</sup>B.-G. Kim, S. Lee, and T. Kishi, *NDT & E Int.* **29**, 317 (1996).

<sup>3</sup>D. Lescribaa and A. Vincent, *Surf. Coat. Technol.* **81**, 297 (1996).

<sup>4</sup>R. Kazys, L. Mazeika, and R. Rausutis, *Proceedings of the 11th International Symposium*, Berlin, Germany, 2002 (Springer, New York, 2002), p. 107.

<sup>5</sup>C. Fritsch and A. Veca, *Ultrasonics* **42**, 797 (2004).

<sup>6</sup>J. Martinsson, F. Hagglund, and J. E. Carlson, *Ultrasonics* **48**, 427 (2008).

<sup>7</sup>L. M. Brekhovskikh, *Waves in Layered Media* (Academic, New York, 1980), Vol. 2, p. 49.

<sup>8</sup>W. C. Chew, *Waves and Fields in Inhomogeneous Media*, *IEEE Press Series on Electromagnetic Waves* (IEEE, New York, 1990), pp. 49–52.

<sup>9</sup>J. Krautkramer and H. Krautkramer, *Ultrasonic Testing of Materials*, 4th ed. (Springer-Verlag, Berlin, 1990), pp. 498–506.

<sup>10</sup>J. Vishnuvardhan, C. V. Krishnamurthy, and K. Balasubramaniam, *Smart Mater. Struct.* **16**, 1639 (2007).